2005 International Symposium on Nonlinear
Theory and its Applications (NOLTA2005)
Bruges, Belgium, October 18-21, 2005

# How ears go electronic

R. Stoop *, A. Kern *, J.-J. v.d. Vyver *

* Institute of Neuroinformatics, University / ETH Zürich, 8057 Zürich
Email: ruedi@ini.phys.ethz.ch

**Abstract**—We demonstrate the design and performance of an artificial Hopf-type electronic cochlea along biomorphic biophysically detailed principles. From a biophysically detailed model of the mammalian cochlea, we first derive a biomorphic close-to-hardware software simulation that is used as the hardware blueprint. By virtue of its biomorphic design, the hardware implementation yields results that are hardly distinguishable from physiological measurements, at a minimum of implementation costs. Moreover, the silicon cochlea shares all the signal processing features exhibited by the biological cochlea. In particular, it may be actively tuned, towards objects provided by an analysis of the auditory scene. With these properties it can serve as the central ingredient for overcoming the well-known cocktail-party problem of hearing.

## 1. Introduction

Understanding hearing is a long-standing human endeavour. The first basic step in understanding the cochlea (the mammalian hearing organ) was achieved by H.L.F. Helmholtz, who suggested the cochlear tonotopic principle to hold (1863 [1]). Von Békésy's discovery of traveling waves along the basilar membrane (BM) within the cochlea (1928 [2]) and Gold's conjecture of active amplification in the cochlea (1948 [3]) were the following landmarks, where the latter was evidenced by the discovery of otoacoustic emissions (1978 [4]), the autonomous sound generation mechanism by the cochlea itself. Since then, various experiments revealed that the locus of active amplification is in the outer hair cells (OHC) residing on top of the basilar membrane [5-6]. Recently, cells homologous to mammalian hair cells were shown to display active, Hopf-type amplification [7-8].

For auditory modeling, Eguíluz et al. [9] proposed in their seminal paper to include Hopf amplifiers as the basic elements. They argued that these nonlinear elements could correctly capture the basic phenomena of hearing: Compression of the dynamic range, sharper tuning for lower intensity sounds, and the generation of combination tones (see also [10]). Here, we demonstrate the final biomorphic electronic realization of this concept. Departing from our previous theoretical cochlea model, we show that the responses obtained from the electronic realization are hardly distinguishable from biophysical measurements.

## 2. The Hopf-cochlea differential equation

In the cochlea, mediated by the cochlear fluid, incoming sound pressure variations transform into incompressible and inviscid hydrodynamic waves that move along the BM [11], causing small BM displacements. Using $x$ to denote the distance from the stapes along the unrolled cochlea, the system can be linearly described by a water-surface wave that is endowed with a surface mass density $m$ and exponentially decreasing transversal stiffness [12] $E(x) = E_0 e^{-\alpha x}$. According to this theory, the wave group velocity $v_G$, the wave vector $k$, and the stationary energy density distribution $e(x, \omega)$, satisfy the relation [13]

$$v_G = \frac{\partial \omega}{\partial k} = \frac{E(x)\rho}{2\omega} \frac{kh + \sinh(kh)\cosh(kh)}{(mk\sinh(kh) + \rho\cosh(kh))^2}. \quad (1)$$

Characteristic frequencies $\omega_c(x)$ correspond to BM locations $x = x_c(\omega)$ of maximal (passive) displacements according to

$$\omega_c(x) = \sqrt{E(x)/m} \quad (2)$$

(which defines the *first tonotopic map*) [13]. It can be shown that $k(x, \omega)$ diverges as $\omega$ approaches $\omega_c(x)$ and that, as $x$ approaches $x_c(\omega)$ for fixed $\omega$, the traveling wave stalls ($v_G = 0$) at the point of (passive) resonance. Due to dissipative losses, the wave amplitude will reach a maximum at $x < x_c(\omega)$, which, consistently with von Békésy's original observations, defines a *second tonotopic map* [13]). From the energy balance equation [14] valid for linear and nonlinear waves alike, $\frac{\partial e}{\partial t} + \frac{\partial}{\partial x}(v_G e) = 0$ and using the ansatz for the energy density $\frac{\partial e}{\partial t} =: -a + de$, the cochlea differential equation emerges as [13]

$$\frac{\partial e}{\partial x} = \frac{-1}{v_G(x,\omega)} \left[ \frac{\partial v_G(x,\omega)}{\partial x} + d(x,\omega) \right] e + \frac{a(x,e,\omega)}{v_G(x,\omega)}. \quad (3)$$

In this equation, the power $a(\cdot)$ locally supplied by the active Hopf amplification, works against the internal viscous losses ($d(x, \omega) = 4\nu k(x, \omega)^2$, where $\nu$ is the kinematic viscosity [15]). In accordance with the biological example, the active amplification results from an array of Hopf-type power sources along the BM, that have varying natural frequencies $\omega_{ch}(x)$. Given a forcing frequency $\omega$, the Hopf amplifiers with $\omega_{ch}(x) \approx \omega$ are maximally excited at locations $x_{ch}(\omega) < x_c(\omega)$, before viscosity leads to a precipitous decay of the wave amplitude.

## 3. Hopf nonlinearity

The characteristics of the active contribution $a$ are derived from a $\omega_{ch}$-rescaled Hopf differential equation

$$\dot{\mathbf{z}} = (\mu + j)\,\omega_{ch}\mathbf{z} - \omega_{ch}\,|\mathbf{z}|^2\,\mathbf{z} - \omega_{ch}\mathbf{F}(t), \quad \mathbf{z} \in \mathbb{C}. \quad (4)$$

Assuming a 1:1 locking between signal and system, $z(t) = Re^{i(\omega t+\theta)}$ is the amplified external periodic input $\mathbf{F} = Fe^{i\omega t}$, $\omega_{ch}$ is the natural frequency of the oscillation, and $\mu \in \mathbb{R}$ denotes the Hopf nonlinearity parameter. With zero external forcing, (4) describes the generic differential equation displaying a Hopf bifurcation: For $\mu < 0$, the solution $z(t) = 0$ is a stable fixed point, whereas for $\mu > 0$, the fixed-point solution becomes unstable and a stable limit-cycle of the form $z(t) = \sqrt{\mu}e^{i\omega_{ch}t}$ appears.

A nonzero forcing $\mathbf{F}$ yields $\omega_{ch}Fe^{-j\theta} = (\mu + j)\,\omega_{ch}R - \gamma\omega_{ch}R^3 - j\omega R$. Squaring and introducing $\phi = \frac{\omega}{\omega_{ch}}$ results in

$$F^2 = \gamma^2R^6 - 2\gamma\mu R^4 + \left[\mu^2 + (1-\phi)^2\right]R^2, \quad (5)$$

which is easily solvable. For $\mu = 0$ and close to resonance $\omega = \omega_{ch}$, the response $R = F^{1/3}$ emerges, which forces the gain $G = R/F = F^{-2/3}$ to increase towards infinity as $F$ approaches zero. This implies a compressive nonlinearity, for any stimulus size. For $\mu < 0$, maintaining $\omega = \omega_{ch}$, we obtain the response $R = -F/\mu$ for weak stimuli $F$. As $F$ increases, the term $R^6$ in Eq. (5) can no longer be neglected, and, as $\gamma R^6 \approx \mu^2R^2 + 2\gamma\mu R^4$, the compressive nonlinear regime is entered. The transition point occurrs at $F_C \approx 0.91(-\mu)^{\frac{3}{2}}/\gamma^{\frac{1}{2}}$. For weak stimuli $F$, the response $R$ is nearly linear, while for moderate stimuli the differential gain of the system, $dR/dF$, decreases with increasing stimulus intensity. Away from the resonance, the last term in (5) dominates. In this case, the response is linear for every input, as $R \approx F/|1-\phi|$. For $\mu > 0$, stable limit-cycles emerge.

In the biological cochlea, the tensile forces acting on the stereocilia tip links, can be considered as the input $\mathbf{F}(t)$ to the Hopf system Eq. (4). Using the equipartition principle, the BM amplitude $A$ has the form $A(x,\omega) = (2e(x,\omega)/E(x))^{1/2}$. For an ensemble of Hopf oscillators active at location $x$, the force amplitude will be proportional to $R$ and have the form $a(e,x,\omega) = L(R(\sqrt{\sigma e(x,\omega)}))^2$, where $L$ and $\sigma$ are proportionality constants [13]. The last two relations establish the connection between our cochlea ODE and physiological measurements.

## 4. Circuit design

Via direct simulations of the differential equation, results for stationary inputs are obtained that are very close to those by the physiological example [13]. For transient signals, however, the equation is beyond usability, due to the computational demand. To remedy this situation, we decomposed the cochlea into sections of characteristic frequencies, each of which is endowed with models of the passive hydrodynamic behavior and of the active Hopf-type amplification. An electronically implemented steady state approximation of the driven Hopf amplifier in combination with a simple fluid transfer function (implemented as a frequency-specific filter), is used as the skeleton of our implementation. The major challenge of our approach is to first properly connect the passive/active components towards a section, and then the latter towards a cascade, now modelling the entire cochlea.

**Hopf part:** The Hopf equation (4) can be approximated in circuitry using a combination of integrative summers and multipliers [17]. Using $\mathbf{v_z} = v_x + jv_y$, the equations

$$\dot{\mathbf{v}}_\mathbf{z} = \left(\frac{-v_\mu}{mCR_\mu} + \frac{j}{CR_\omega}\right)\mathbf{v_z} - \frac{|\mathbf{v_z}|^2\mathbf{v_z}}{2m^2CR_\gamma} - \frac{\mathbf{v_F}}{CR_F}, \quad (6)$$

are obtained. $\mathbf{v_F}$ denotes the input amplitude and $v_\mu$ the control parameter; the multiplier $m$ is implemented by means of analog multipliers (according to $v_o = \frac{v_{i_0}\cdot v_{i_1}}{m}$). To map the Hopf system on the circuit, the uncompressed interval should be identified, and mapped on the non-saturation regime $V_{CC}$ of the op-amp. We chose this interval as $I_F = [0^+, F_C(\mu^*)]$, where $\mu^*$ is a sufficiently negative value of $\mu$ where $\log[F_C]$ does not substantially increase anymore, For the proper mapping, we write $\mathbf{v_z} = A_z\mathbf{z}$, $\mathbf{v_F} = A_F\mathbf{f}$, $v_\mu = A_\mu\mu$. From equating (6) with (4), we obtain

$$\dot{\mathbf{z}} = \left(\frac{-A_\mu\mu}{mCR_\mu} + \frac{j}{CR_\omega}\right)\mathbf{z} - \frac{A_z^2|\mathbf{z}|^2\mathbf{z}}{2m^2CR_\gamma} - \frac{A_F\mathbf{f}}{CR_FA_z}. \quad (7)$$

The mapping thus requires to use $A_F \gg V_{CC}/F_C$. We chose $A_F = V_{CC}$. To obtain a unitary gain, we set $A_z = A_F$. $A_\mu$, finally, could be set arbitrarily, but is naturally chosen as $A_\mu = -V_{CC}/\mu$. In order to treat properly situations where $\mu$ is changing over an interval $I_\mu$, we replace $\mu$ by $\min(I_\mu)$. At given capacitance $C$, the resistor values are then calculated from the equivalence between (4) and (7) to

$$R_\omega = \frac{1}{C\omega_{ch}},\ R_\mu = \frac{-A_\mu}{mC\omega_{ch}},\ R_f = \frac{A_F}{A_zC\omega_{ch}},\ R_\gamma = \frac{A_z^2}{2m^2C\gamma\omega_{ch}}, \quad (8)$$

$\omega_{ch} > 0$. $\phi$ plays the same role as in linear filters: It relates the response curves to the characteristic frequency, see Figs. 2,3. Unlike linear filters, which are only dependent upon the normalized input frequency $\phi$, the Hopf amplifier response is also influenced by the input amplitude $F$. Furthermore, the response can be controlled by adjusting $\mu$. The linear gain, at the characteristic frequency, for small input signals is preserved by this scaling, as is the compressive gain with exponent $-2/3$ for increased input signal strength.

To support an intuitive understanding of the circuit, we note that the Hopf equation (4) with nonzero driving can be interpreted as a nonlinear filter, with a tunable gain control ("quality factor") $|\mu|$ and an envelope detector $|\mathbf{z}|^2$. As the bandwidth $\Gamma \sim |\mu|$ for $F \le F_C$ (and $\Gamma \sim \gamma^{\frac{1}{2}}F^{\frac{2}{3}}$ for $F > F_C$), small $|\mu|$-values act as a high Q-factors (sharp resonances).

**Passive part:** As is suggested by the response generated by the Hopf cochlea differential equation, the passive part can be modeled as a 6th-order Butterworth circuit. For reasons of hardware availability, the 6th-order Butterworth equation was separated into three 2th-order low pass filters (see Fig. 1). The rescaled, centered around unity, section input frequency $\phi$ will then be transformed according to

$$B_6(\phi) = \sum_{i=0}^{6} \frac{1}{a_i \phi^i} = \frac{1}{(\phi^2+0.518\phi+1)} \cdot \frac{1}{(\phi^2+\sqrt{2}\phi+1)} \cdot \frac{1}{(\phi^2+1.932\phi+1)}. \quad (9)$$

The first filter has a gain in excess of 1 at the characteristic frequency. Thus, at large input voltages and small control values, saturation of the op-amps will occur. This problem can be compensated for by changing the order of the 2th-order circuits or by constructing a single 6th-order circuit. We chose the first option. As the characteristic frequency of the Hopf amplifier is higher than that of the Butterworth filter and hence the amplification of small signals takes place earlier, this choice should not even affect the processing of very small inputs.

**The Cochlea:** is implemented as a cascade of sections. Classical feedback and open-loop gain amplifications run into the problem of getting the phases of the passive and the active behavior to interact constructively. Therefore, and since the passive component is described as a signal transformation (instead of signal propagation), a simplified feedforward coupling scheme is used for the connection between the active and the passive components. Not only does this require less components, its behavior is easier to assess, as phase and delay information can be ignored. Following these principles, a circuit was designed, translated into Simulink and built in hardware, see Fig. 1.

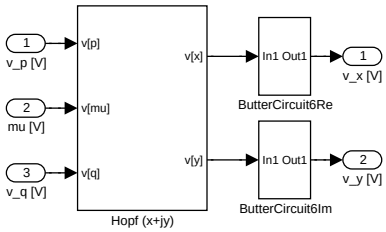


Figure 1: Circuit diagram of a section, consisting of a Hopf amplifier and two 6th-order Butterworth filters.

If, as an example, the values $\omega_{ch} = 500\,[s^{-1}]$, $\gamma_0 = 10^8$, and $\mu \in \{-10^3, -10^2, -10, -1\}$ are chosen, this leads to $F_C(\mu) \in \{3.1623, 0.1, 0.0031623, 0.0001\}$, respectively. From the Hopf Eq. (4), it can be inferred that $\max|\mu| = 1000$, $\max|F| = 1$, $\max|z| = 0.00225$, which leads to $A_\mu = -0.01$, $A_F = 10$, $A_z = 4444.4$. Choosing $C = 10^{-6}\,[F]$ yields $R_\omega = 2000$, $R_\mu = 10000$, $R_F = 0.00225$, $R_\gamma = 987.63\,[\Omega]$. Using the TL082CP and the AD734AN chips, this leads to $m = 10$ in (6-8).

To parametrically describe the design of a generic section, thus the detuning between the passive frequency $\omega_s$ and the Hopf amplifier frequency $\phi_s(i) := \omega_s(i)/\omega_{ch,s}(i) < 1$, $i = 1, \ldots, n$, where $n$ is the number of sections, is sufficient. This is our first design parameter. The second design parameter is the relationship between the characteristic frequencies of subsequent section frequencies

$$\Psi(i) = \frac{\omega_s(i+1)}{\omega_s(i)}, \quad i = 1 \ldots n-1. \quad (10)$$

In the following, we will chose the two parameters independent from the section, as $\Psi(i) = \Psi, \phi_s(i) = \phi_s, \forall i$. The design of a generic cascade element, the section, is now fully described in terms of these two parameters. The system is modeled in Matlab Simulink as an ideal circuit, using the chosen capacitance and calculated resistance values. The Hopf amplifier is put "in front" of the passive unit, because of the feedforward coupling of the active amplification [13]. Connecting sections in series, finally, builds up the cochlear cascade.

## 5. Measurements

In addition to verifying hardware concepts before going in print, the Simulink model can be used to investigate the time evolution of the Hopf amplifier. We report here only on the steady state circuit response (transient signals add no particular problems). For this case, regular analysis techniques need to be slightly adapted. Since both the input and output represent complex values, the signal amplitude is the absolute value of the complex description. Design parameters, which lead to a span of one octave for a small number of sections, are $\phi_s = 1.05^{-1}$ and $\Psi = 0.84$.

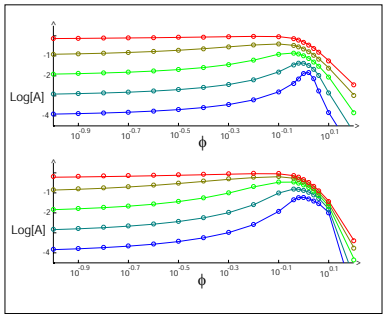


Figure 2: Output from one section and a two-section cochlea. Circles denote measurements, the solid line the corresponding values from the Simulink model. Additional sections modify the local structures.

**1 and 2-sections cochlea :** The degree of match between Simulink simulations and the actual circuits was checked at different relevant parameter values and found to be very good. For the above setting, in Fig. 2 the basilar membrane velocity was measured for varying input frequency at a fixed place, for different stimulation strengths. In all aspects, measurements and simulations of the one and

two-section circuits correspond very well with the original model Eq. (3), in particular perfectly reproducing as the key feature the compressive nonlinearity of the mammalian cochlea.

**Comparison software-hardware-biology:** By increasing the number of the sections, the soft- and hardware models can be made to ever better approach the behavior of the mammalian cochlea. For the latter, the basilar membrane velocity is measured against the input frequency at a fixed measuring place, for different stimulation strengths. The comparison of 5 sections soft- and hardware vs. the mammalian bioware, is shown in Fig. 3. In the software simulation, a discretization effect induced by the small number of sections vs. the large frequency span is observed. Generally, the discrepancies between hardware measurements and software simulations were found to be below 10% of the measured signals. The strength of the discretization effect is a function of the frequency distance between ajacent sections ($\Psi$) and resonance widths of the active amplifiers, which are a function of the chosen $|\mu|$-values. The smaller this size, the more discretization features are observed. Simple calculations imply that an array of $\sim 30$ sections will lead to a hearing sensor that is hardly distinguishable from the mammalian hearing organ.

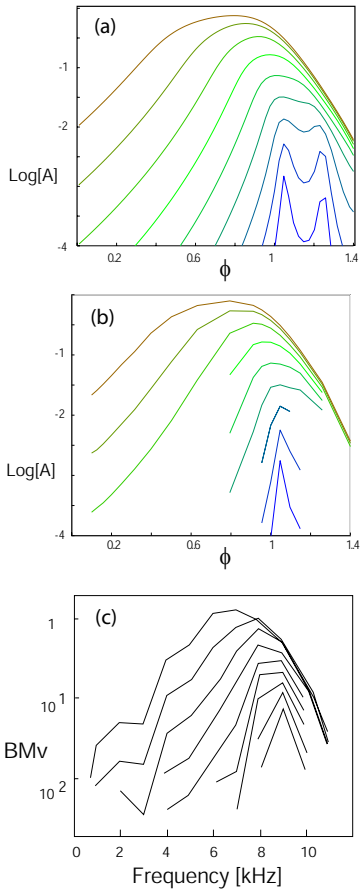


Figure 3: Comparison between 5-section soft-, hardware and the mammalian cochlea (chinchilla, Ruggero [18]), a), b), c), respectively. In a), the two-humped resonance for small inputs is a discretization effect that vanishes if more sections are chosen (e.g., $n = 7$), or if $\mu$, which determines the bandwidth $\Gamma$ ($\sim |\mu|$, below $F_C$), is increased. Fortunately, in the mammalian cochlea, $\Gamma$ is relatively large.

## References


[1] H.L.F. Helmholtz, *Die Lehre von den Tonempfindungen als physiologische Grundlage für die Theorie der Musik* (Vieweg, Braunschweig, 1863).

[2] G. von Békésy, "Zur Theorie des Hörens. Die Schwingungsform der Basilarmembran", *Phys. Z.*, vol. 29, pp. 793–810 (1928).

[3] T. Gold, "The physical basis of the action of the cochlea", *Proc. R. Soc. Lond. B*, vol. 135, pp. 492–498 (1948).

[4] D.T. Kemp, "Stimulated accoustic emission from within the human auditory system", *J. Acoust. Soc. Am.*, vol. 64, pp. 1386–1391 (1978).

[5] W.E. Brownell, C.R. Bader, D. Bertrand, Y. de Ribaupierre, "Evoked mechanical responses of isolated cochlear outer hair cells", *Science*, vol. 227, pp. 194–196 (1985).

[6] L. Robles, M.A. Ruggero, "Mechanics of the mammalian cochlea", *Physiol. Rev.*, vol. 81, pp. 1305–1352 (2001).

[7] P. Martin, A.J. Hudspeth, "Compressive nonlinearity in the hair bundel's active response to mechanical stimulations", *Proc. Natl. Acad. Sci. U.S.A.*, vol. 98, pp. 14386–14391 (2001).

[8] M.C. Göpfert, A.D.L. Humphris, J.T. Albert, D. Robert, O. Hendrich, "Power gain exhibited by motile neurons in *Drosophila* ears", *Proc. Natl. Acad. Sci. U.S.A.*, vol. 102, pp. 325–330 (2005).

[9] V.M. Eguíluz, M. Ospeck, Y. Choe, A.J. Hudspeth, M.O. Magnasco, "Essential nonlinearities in hearing", *Phys. Rev. Lett.*, vol. 84, pp. 5232–5235 (2000).

[10] S. Camalet, T. Duke, F. Jülicher, J. Prost, "Auditory sensitivity provided by self-tuned critical oscillations of hair cells", *Proc. Natl. Acad. Sci. U.S.A.*, vol. 97, pp. 3183–3188 (2000).

[11] E. de Boer, "Mechanics of the cochlea: Modelling efforts", in *The Cochlea. Springer Handbook of Auditory Research*, P. Dallos, A.N. Popper, R.R. Fay, Eds. (Springer, New York, 1996), pp. 258–317.

[12] B.P. Peterson, L.C. Bogert, "A dynamical theory of the cochlea", *J. Acoust. Soc. Am.*, vol. 22, pp. 369-381 (1950).

[13] A. Kern, R. Stoop, "Essential role of couplings between hearing nonlinearities", *Phys. Rev. Lett.*, vol. 91, pp. 128101 1–4 (2003).

[14] G.B. Whitham, *Linear and Nonlinear Waves* (Interscience Publishers, New York, 1999).

[15] J. Lighthill, *Waves in Fluids* (Cambridge University Press, Cambridge, 2002).

[16] R.J. Smith, R.C. Dorf, *Circuits, Devices ans Systems* (John Wiley & Sons, 1991).

[17] M.A. Ruggero, "Responses to sound of the basilar membrane of the mammalian cochlea", *Curr. Opin. Neurobiol.*, vol. 2, pp. 449–456 (1992).